Proceedings of 12th European Conference on Turbomachinery Fluid dynamics
Paper ID: ETC2017-324 & Thermodynamics ETC12, April 3-7, 2017; Stockholm, Sweden

Time resolved PIV measurements of the unsteady wake migration in a LPT blade passage: effect of the wake passing frequency

D. Lengani D. Simoni M. Ubaldi P. Zunino

DIME - Universitá di Genova, Via Montallegro 1, I-16145 Genoa, Italy

F. Bertini

GE Aviaero SRL, Torino, Italy

ABSTRACT

A time resolved Particle Image Velocimetry (TR-PIV) system has been employed to investigate the unsteady propagation of upstream wakes in a low-pressure turbine cascade. Data are obtained in the steady state condition and for two passing wake reduced frequencies. The study is focused on the identification and split of the different dynamics responsible for deterministic and random oscillations, thus loss generation. A very large data set has been collected: for each condition, about 9000 instantaneous flow fields have been acquired at up to 2kHz in order to resolve with great detail the vortex shedding phenomenon characterizing the separation at steady condition as well as the propagation of the coherent structures induced by the incoming wake. Instantaneous vector maps, phase averaged velocity fields and Proper Orthogonal Decomposition (POD) have been used for the in depth characterization of the different phenomena.
The paper takes advantage of the properties of POD that reduces the data set to a low number of modes that represent the most energetic dynamics of the system. It is clearly shown that the phase averaged flow field can be represented by a few number of POD modes related to the wake passing event for the unsteady cases. POD is also able to capture flow features affecting the instantaneous flow field not directly related to the wake passage (i.e. the vortex shedding phenomenon induced by the intermittent separation developing between adjacent wakes), that are smeared out in the phase averaged results. Once recognized the POD modes most involved in the unsteady flow field, a procedure for the quantification of the different contributions to the overall amount of losses is proposed.

INTRODUCTION

The flow field in turbomachinery blade rows is significantly affected by the deterministic oscillations due to the rotor-stator interaction process. Literature of the last 20 years clearly highlights that in low pressure turbine (LPT) rows incoming passing wakes generate a jet like structure that, impinging on the blade suction side, opens in two branches generating two large scale coherent structures (e.g. **?**Hodson and Howell 2005). The turbulence activity carried by these large scale vortices increases during migration, being the wake region stretched and bowed by the cascade pressure field. Consequently, wake migration contributes to the loss generation by its self (Michelassi et al, 2015), as well as through the alteration of the boundary layer transition and separation (if any) processes (e.g. Lengani et al 2016). In this respect, the anticipation of the boundary layer transition contributes to delay or suppress the separation process that may occur on high lift profiles operating at low Reynolds number condition. Detailed URANS calculations are able to describe the evolution of the periodic part of the unsteady motion, but provide only the statistical evolution of the turbulent activity (e.g., Pacciani et al 2012). Similarly, the phase-averaged treatment of experimental data allows the detailed analysis of the periodic flow due to the wake, while the random part of flow oscillations can be only statistically described (Satta et al, 2014). In both cases all the unsteadiness sources not directly related to the wake passing frequency are not resolved, and their role in the loss generation mechanisms

remains substantially obscure.

In the present paper TR-PIV measurements describing the flow field in a highly loaded LPT cascade have been analyzed with the aim of identifying, splitting and characterizing the different phenomena producing losses. To this end, POD has been applied to the instantaneous flow fields characterizing the steady state, and two different incoming wake reduced frequencies. For the steady case POD has been proved to be able to identify structures associated with a by-pass like transition process (Lengani and Simoni, 2015) as well as the coherent structures shed as a consequence of the boundary layer separation (Lengani et al, 2014; Kurelek et al, 2016). On the other hand, in the unsteady case the most energetic POD modes well describe the spatial structure of the negative jet and the related large scale vortices attached to the leading and trailing boundary of the wake (see Sarkar 2008; Lengani et al 2016). In the present work POD mode distributions and related temporal coefficients are compared with time resolved and phase-averaged velocity fields in order to provide a clear evidence of the physical meaning of each mode, and the flow dynamics it represents. The effects of the reduced frequency variation (from the steady state to the nominal unsteady condition) on the main dynamics inducing flow oscillations (i.e. boundary layer separation, and incoming wake effects) will be deeply characterized by means of POD modes and related temporal coefficients. Additionally, taking care of the bi-orthonormality of POD modes and the corresponding temporal coefficients the contribution of each mode to both the normal and the shear Reynolds stresses is identified. The combination of the Reynolds stresses and the local flow distortion allows the computation of the loss generation rate per mode. This allows the identification and split of the role played by the different superposed phenomena on the overall amount of losses.

Nomenclature

C	blade chord
f_{bar}	bar passing frequency
f^+	wake reduced frequency = $f_{bar}C/u_{2,is}$
g	pitch
h	blade height
LP	low pressure
Re	Reynolds number = $Cu_{2,is}/\nu$
s	curvilinear coordinate
s_{MAX}	trailing edge curvilinear coordinate
t	time
T	wake passing period
u	streamwise velocity component
$u_{2,is}$	isentropic velocity at cascade outlet
$u_{2,x}$	axial velocity at cascade outlet
U_0	inlet streamwise velocity
U_{bar}	bar rotation velocity
v	normal to the wall velocity component
x	cascade axial coordinate
y	normal to the wall direction
δ	boundary layer thickness
$\lambda^{(k)}$	POD eigenvalue of mode k
$\chi^{(k)}$	POD eigenvectors of mode k
φ	flow coefficient = $u_{2,x}/U_{bar}$
ϕ_u	POD mode of the streamwise velocity component
ϕ_v	POD mode of the wall normal velocity component
$<>$	deterministic periodic component

Subscripts & Superscripts

RMS	root mean square
$-$	time averaged quantities
$\sim$	phase-locked quantities
$'$	stochastic fluctuating component

EXPERIMENTAL APPARATUS AND DATA REDUCTION

Test facility and instrumentation

The experimental investigations have been performed in a blow-down wind tunnel installed at the Aerodynamics and Turbomachinery Laboratory of the University of Genova. The test section is constituted of a 7 blades large scale planar cascade (Fig. 1), representative of highly loaded LPT blade profiles. Blades are characterized by a chord length of 120 mm and an aspect ratio AR = 2.5 to ensure two-dimensional flow at midspan. Measurements have been carried out at a low Reynolds number condition Re = 70000 with both steady and unsteady incoming flow. The inlet free-stream

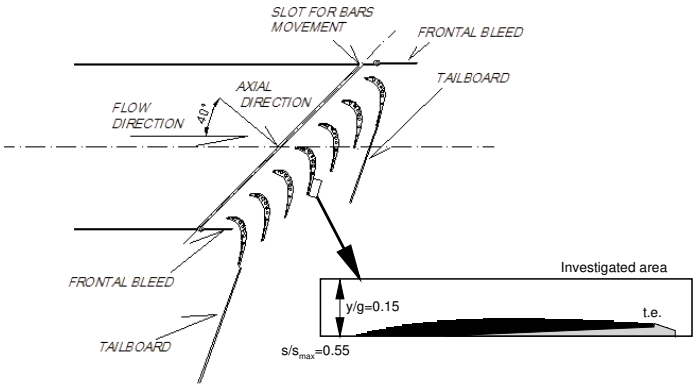

Figure 1: **Sketch of the test section and PIV investigated area.**

turbulence was Tu = 4.2%.

Upstream wakes have been simulated by means of a tangential wheel of radial rods. The flow coefficient was set to $\varphi = 0.675$ to be representative of real engine operative conditions. Two different reduced frequencies have been analyzed ($f^+ = 0.69$ and $f^+ = 0.35$) referred in the following as nominal and halved condition, respectively.

PIV measurements have been performed in order to characterize the unsteady transition process of the suction side boundary layer perturbed by upstream wakes. The PIV field of view (Fig. 1) covers the flow region $0.55 < s/s_{max} < 1.1$ and $0.0 < y/g < 0.15$. In this region about 9000 couples of images have been acquired in order to obtain high statistical accuracy. A data set at a lower acquisition frequency and with a larger extension in the pitchwise direction ($0.0 < y/g < 0.46$) has been also acquired for the nominal reduced frequency case for a better characterization of the wake migration in the potential flow region.

The light source is a dual-cavity Nd:YLF pulsed laser Litron LDY 300 (energy 2x30 mJ per pulse at 1000 Hz repetition rate, 527 nm wavelength). The optical system forms a light sheet of 1 mm thickness. The light scattered by the seeding particles (vaseline oil droplets with a mean diameter of 1.5 μm) is recorded on a high sensitive SpeedSense M340 digital camera with a cooled 2560 x 1600 pixels CMOS matrix. The camera frame rate has been set to 2000 Hz reducing the field of view of the camera to 2560 x 400 pixels and operating it in double frame mode. The magnification factor for the present experiments was set to 0.285 in order to obtain a high spatial resolution. The cross-correlation function has been calculated over a 16x16 pixels interrogation area with a 50% overlap. This corresponds to a vector spacing of 0.28 mm. With an accuracy of the sub-pixel interpolation of 0.1 pixel, the experimental uncertainty for the instantaneous velocity has been estimated to be 3.0% of the maximum measurable velocity.

Data analysis

The time resolved PIV data have been analyzed by means of proper orthogonal decomposition (POD) in order to highlight dynamics related to the different source of unsteadiness, thus providing new insight into the mechanisms producing losses. The POD (e.g. Lengani et al 2014) provides a triplet of information: the eigenvalues $\lambda^{(k)}$, the eigenvectors $\chi^{(k)}$ and the POD modes $\phi^{(k)}$. The eigenvalue of the k^{th} mode represents the energy contribution of the mode to the total kinetic energy of velocity fluctuations. The eigenvectors constitute an orthogonal basis and retain the temporal information related to each mode. They can be used to provide phase averaged flow field without using an external trigger signal as discussed in Lengani et al (2014), as well as to analyze the characteristic frequency of each structure. The POD modes constitute an orthogonal basis that provides the spatial information identifying coherent structures in the flow.

Since the POD modes and eigenvectors are orthogonal, the Reynolds shear and normal stresses

can be computed, adopting an index notation, as:

$$\overline{u_i' u_j'} = \sum_k \lambda^{(k)} \phi_i^{(k)} \phi_j^{(k)} \tag{1}$$

The term $\lambda^{(k)} \phi_i^{(k)} \phi_j^{(k)}$ represents the contribution of the k^{th} POD mode to the overall time-mean Reynolds stresses. This property of POD can be applied to split the contribution to the TKE production terms P_{TKE}. For 2D flows, in Cartesian notation P_{TKE} assumes the form:

$$P_{TKE} = -\overline{u'^2}\frac{\partial \overline{U}}{\partial x} - \overline{u'v'}\frac{\partial \overline{U}}{\partial y} - \overline{u'v'}\frac{\partial \overline{V}}{\partial x} - \overline{v'^2}\frac{\partial \overline{V}}{\partial y} \tag{2}$$

P_{TKE} represents also the mean flow loss generation rate, since it appears in both the TKE and mean flow kinetic energy transport equations but with reversed sign. Each term appearing in Eq. 2 can be generically represented as:

$$p_{ij} = -\overline{u_i' u_j'}\frac{\partial \overline{U}_i}{\partial x_j} \tag{3}$$

Substituting Eq. 1 in Eq. 3, the contribution of each POD mode to the production rate of each term p_{ij} can be computed as:

$$p_{ij}^{(k)} = -\lambda^{(k)} \phi_i^{(k)} \phi_j^{(k)} \frac{\partial \overline{U}_i}{\partial x_j}, \quad with \quad p_{ij} = \sum_k p_{ij}^{(k)} \tag{4}$$

According to these equations, each POD mode contributes to a quota of the TKE generation rate. Therefore, the contributions to the overall losses due to boundary layer, wake migration and their combination can be split and analyzed separately, thus providing further insight in the mechanisms producing losses.

RESULTS AND DISCUSSION

The time-mean velocity distributions of the steady state and the two unsteady cases are represented in Fig. 2. The steady state condition shows a separated boundary layer with zero velocity in the aft portion of the blade suction side. Conversely, due to the wake effects the boundary layer appears completely attached in the nominal unsteady case. These results confirm the well known beneficial effects of unsteady passing wake in suppressing separation (e.g., Hodson and Howell 2005; Michálek et al 2012). Time-mean boundary layer separation seems to be not present neither for the f^+=0.35 condition, even though lower velocity levels can be observed close to the wall. As it will be discussed in the following, this latter condition is characterized by an unsteady separation, and POD will be shown to clearly capture the dominant dynamics responsible for flow oscillations and losses in the different conditions.

Unsteady flow analysis

Thanks to the high frequency response of the TR-PIV instrumentation, the evolution of the flow field can be directly observed to provide a clear view of the flow unsteadiness and complexity. In Fig. 3 evenly time spaced instantaneous perturbation velocity vector maps, (u',v') according to the Reynolds decomposition, are reported for the case f^+=0.35. The color plots of u' are also superposed to empathize the occurrence of localized low and high speed regions during the wake-boundary layer interaction process. About half of the blade passing period is considered. In the first frame the boundary layer develops unperturbed by the wakes. Large negative values of u' can be observed in the aft portion of the blade suction side, jointly with the occurrence of large scale vortical structures. Due to

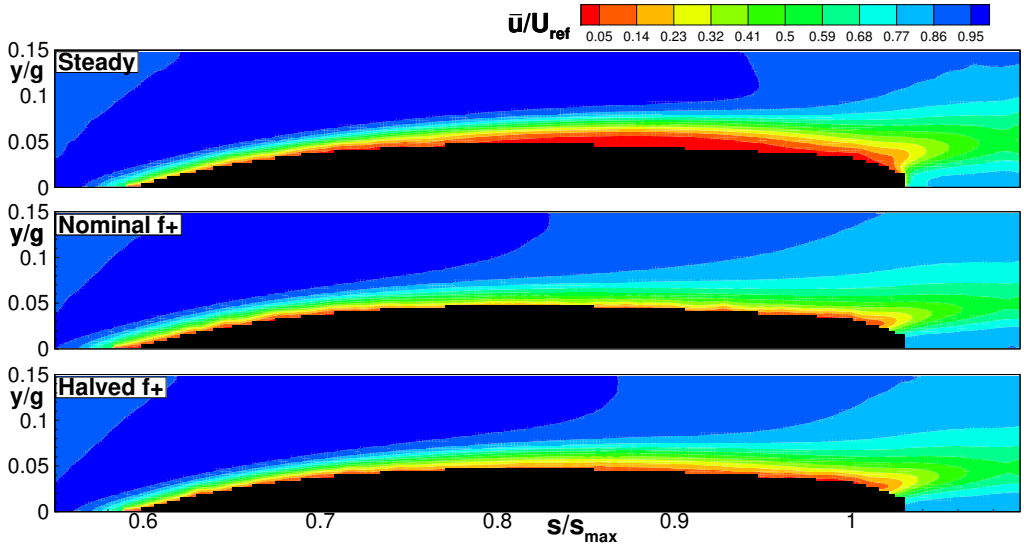

Figure 2: **Time-mean streamwise velocity component, from top to bottom: steady inlet flow case, nominal reduced frequency, halved reduced frequency.**

the low reduced frequency unsteady boundary layer separation occurs between adjacent wakes. The wake is entering the domain at the second time instant, as it can be deduced by the positive values of u' in the fore portion of the suction side away from the wall. While the wake is moving along the former part of the blade (see the second and third images) the separated flow region still sheds vortices. As soon as the wake interacts with the near wall low velocity region roll up vortices originate (see the vector maps in the neighboring of the blue area in the fore portion of the blade in the third and fourth frames). Later the wake moves further downstream and starts interacting with the separated flow region, and the unsteady behavior of the near wall flow becomes extremely complex. Separation is fully suppressed in the sixth and seventh images, where the region close to the wall is characterized by large positive values of u'. In the last frame the flow appears quite ordered even thought the wake is still interacting with the boundary layer, as highlighted by the elevated negative u' values outside the boundary layer region. Wake boundary layer interaction manifests low random oscillations at the end of the interaction process, since the turbulent activity carried by the wake is mainly concentrated at its leading boundary, as described in (Lengani et al, 2016).

The unsteady flow field here observed is clearly characterized by stochastic and deterministic (periodic) events due to roll up vortices and the wake related effects, respectively. Deterministic fluctuations are classically analyzed by means of phase averaged data, which are able to solve the periodic motion but provide only a statistical representation of the stochastic activities (through the phase-locked rms distribution). On the other hand, POD can be used to characterize the spatio-temporal evolution of both deterministic and stochastic phenomena that contribute to the unsteady flow field just observed, as discussed in previous publications (Lengani and Simoni 2015; Lengani et al 2016).

The ability of POD of resolving deterministic events can be appreciated by the comparison between the most energetic POD modes and the phase-averaged flow field. In Fig. 4 and Fig. 5 results for the nominal f^+ case are reported as example. Figure 4 shows the phase-averaged flow evolution for different phases. The contour plot of the purely periodic component ($< u(t) >= \tilde{u}(t) - \overline{u}$, where $\tilde{u}(t)$ is the phase averaged velocity) and the vectorial representation of $< u >, < v >$ are represented in the pictures. The reconstructed phase-averaged velocity field is represented as a plot sequence for 4 phases within a wake passing period. The extended measurement domain is considered to better appreciate the large scale structures induced by the wakes.

The first instant ($t/T = 0.0$) captures the wake entering the measurement domain, since a large scale counter-clockwise rotating vortex is clearly observable in the aft portion of the measuring domain. As described in Gompertz and Bons (2011) it is due to the low momentum wake flow that

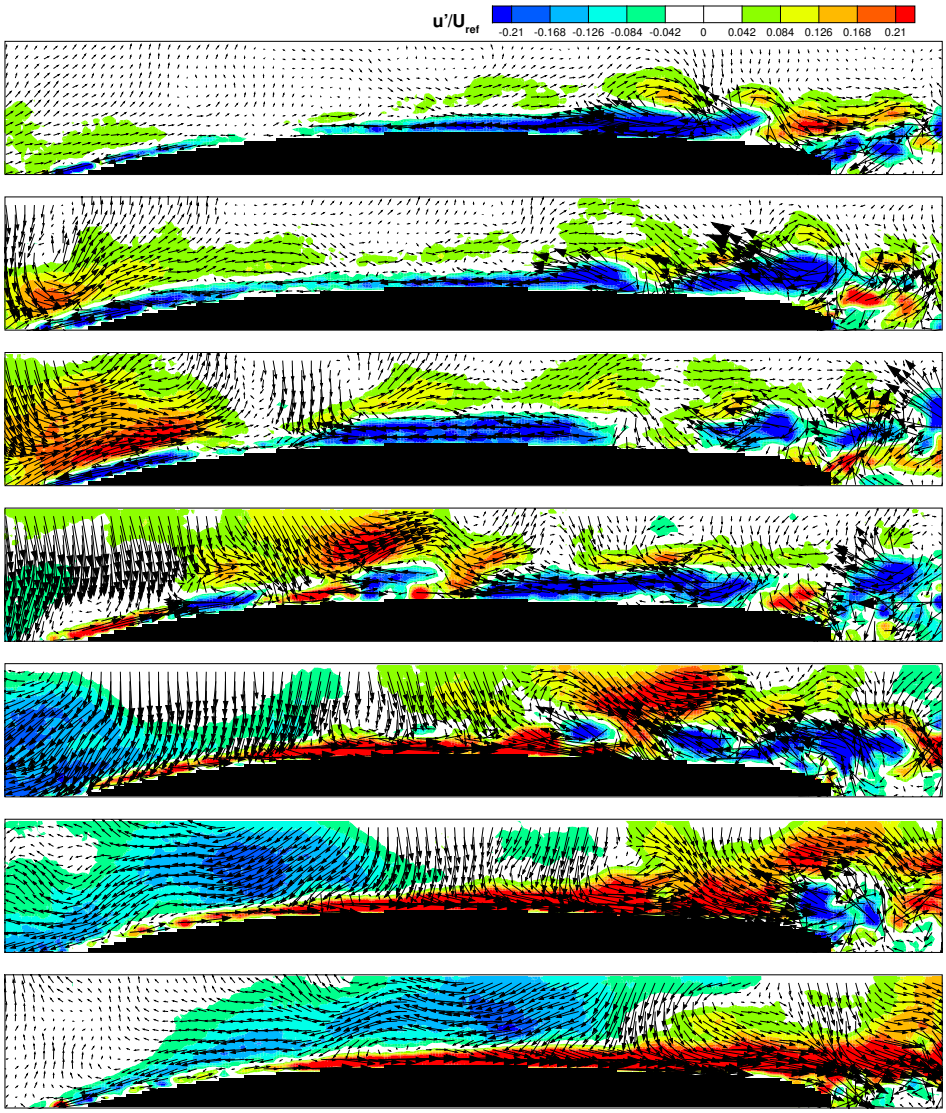

Figure 3: **Time series of the instantaneous perturbation velocity, 0.5 f^+ case. The time interval between each snapshot is 0.06 of the wake passing period (5 times larger than the TR-PIV temporal resolution).**

impinging on the blade surface opens in two branches. The stream at the leading boundary of the wake induces positive values of $< u >$ at the edge of the boundary layer, thus provoking high shear effects and rollup vortices formation. The wake jet structure pointing toward the wall can be clearly recognized at $t/T = 0.25$, while successively the clockwise rotating structure appears as the wake moves further downstream (t/T=0.75).

The most energetic POD modes (Fig. 5 on the left) provide the statistical representation of the large scale structures responsible for the phase-averaged flow field just observed. It is worth noting that the POD modes and all the following pictures concern the boundary layer restricted plane (as depicted in Fig. 1), which is indicated by the black box in Fig. 4 for a fast comparison. The vectorial representation shows the POD mode of the two velocity components. The Fourier analysis of the temporal eigenvector (right of Fig. 5) allows identifying passing wake related modes trough the occurrence of distinct peaks at the wake passing frequency and higher harmonics.

For the nominal reduced frequency the first two POD modes depict the velocity perturbation induced by the large scale structures of the wake on the boundary layer. The first POD mode appears similar to the phase averaged representation at the time t/T=0.75 and the second POD mode to that

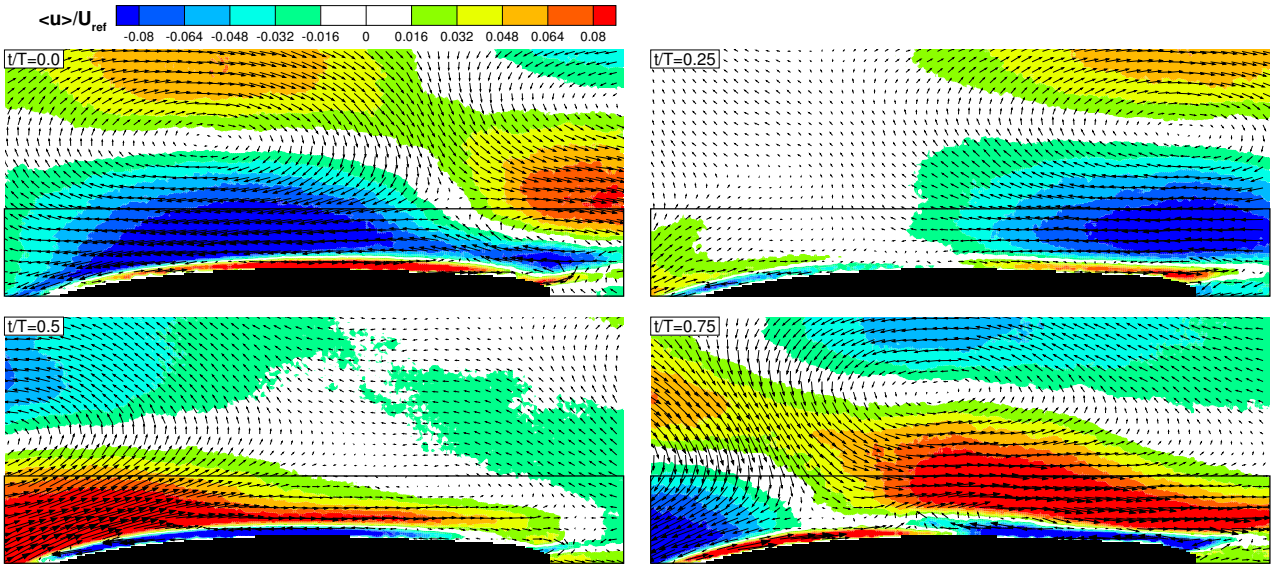

Figure 4: **Phase-averaged velocity vector maps with superimposed the streamwise velocity contour. Nominal f^+**

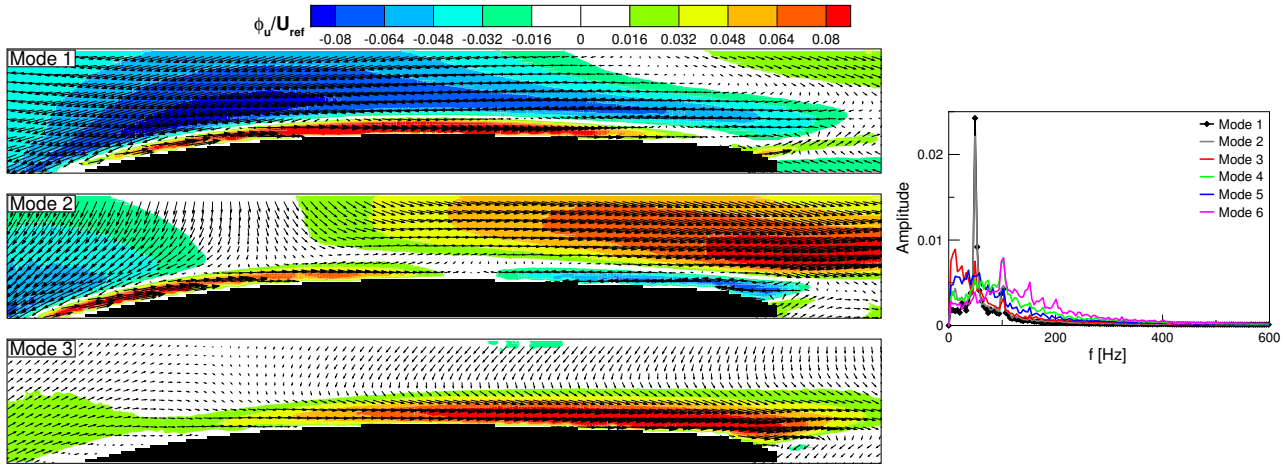

Figure 5: **POD modes (left) and Fourier spectra of POD eigenvectors (right) for the nominal f^+ case.**

at t/T=0.5. The FFTs of their temporal coefficients are almost identical, and clearly show peaks at the wake passing frequency and higher harmonics (the temporal coefficients are two similar periodic waves shifted of 90 deg). The combination of the first two POD modes and the corresponding temporal coefficients provides the reconstructed flow field associated with the periodic motion (i.e. the phase-averaged flow field). Indeed, at the instant when the temporal coefficient of one of the two POD modes is zero, the other mode directly describes the instantaneous periodic flow map. However, the capability of POD goes beyond the identification of passing wake related effects. Indeed, the third mode in Fig. 5 evidently provides the statistical representation of oscillations not observed in the phase averaged flow field. This mode, according to the Fourier analysis, is poorly associated to the wake passing events, and consequently only marginally contributes to the phase-averaged flow field. Modes 3 mainly describes the low frequency velocity fluctuations due to elongated structures contributing to the boundary layer transition process (i.e. streaky structures), similarly to the results shown in a recent authors' publication (Lengani and Simoni, 2015). The POD analysis of the steady cases shown in Fig. 6 makes evident the "boundary layer nature"' of this mode. Indeed the first

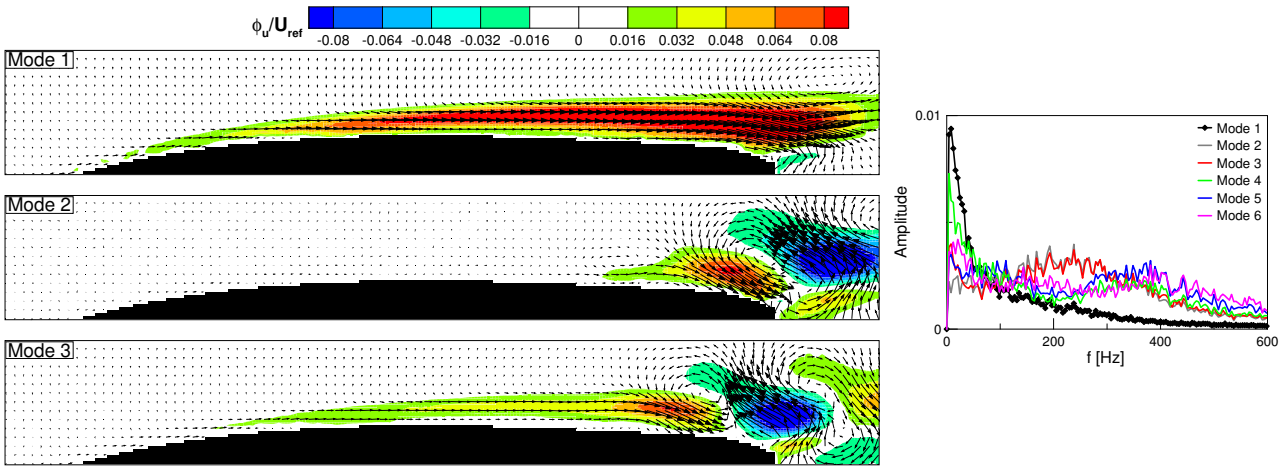

Figure 6: **POD modes (left) and Fourier spectra of POD eigenvectors (right) for the steady case.**

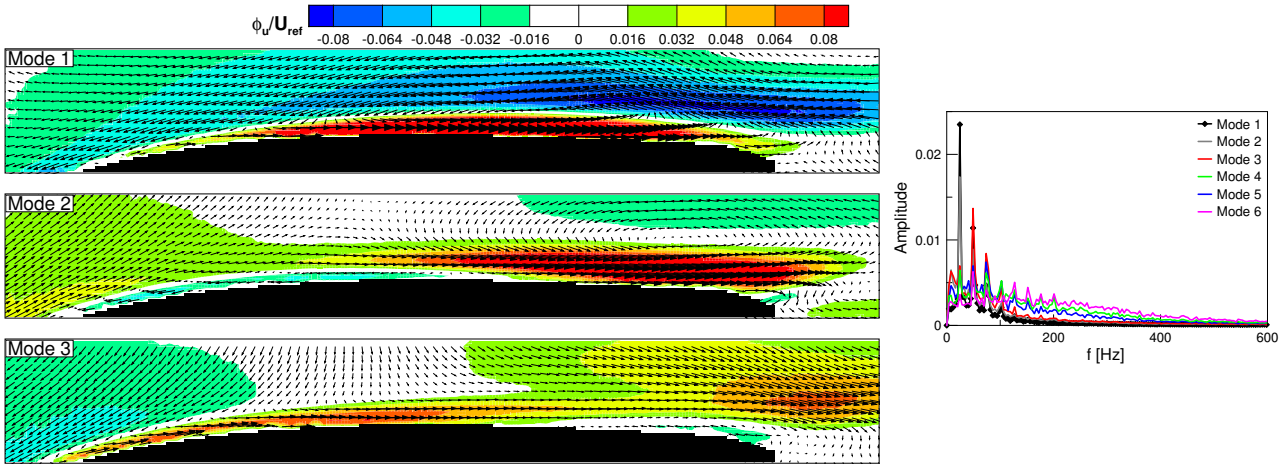

Figure 7: **POD modes (left) and Fourier spectra of POD eigenvectors (right) for the halved f^+ case.**

POD mode of this last case is almost identical to the third mode of the nominal unsteady case. The shape of this mode is the trace of streaky structures inside the suction side boundary layer generating as a consequence of the high free-stream turbulence level, as also observed in [xx]. The following modes represent alternating vortical structures that are characterized by fluctuating energy in a frequency range around 200Hz. These modes provide the statistical representation of the vortical structures shed behind the separation bubble maximum displacement position as a consequence of a Kelvin-Helmholtz instability process. In the steady case the most energetic oscillations are due to low frequency activity and the vortex shedding phenomenon, and POD clearly identifies and isolates also these mechanisms. No oscillations can be observed far from the wall since only the homogeneous free stream turbulence travels across the potential flow region.

For completeness the POD modes and the Fourier analysis of the eigenvectors is also reported for the halved reduced frequency condition in Fig. 7. The first mode is similar to the first mode of the nominal reduced frequency case, while the second mode resembles the low frequency activity boundary layer mode. Now is the third mode that become representative of the wake jet structure, similarly to mode 2 for the nominal frequency. Indeed, due to larger distance between successive wakes a

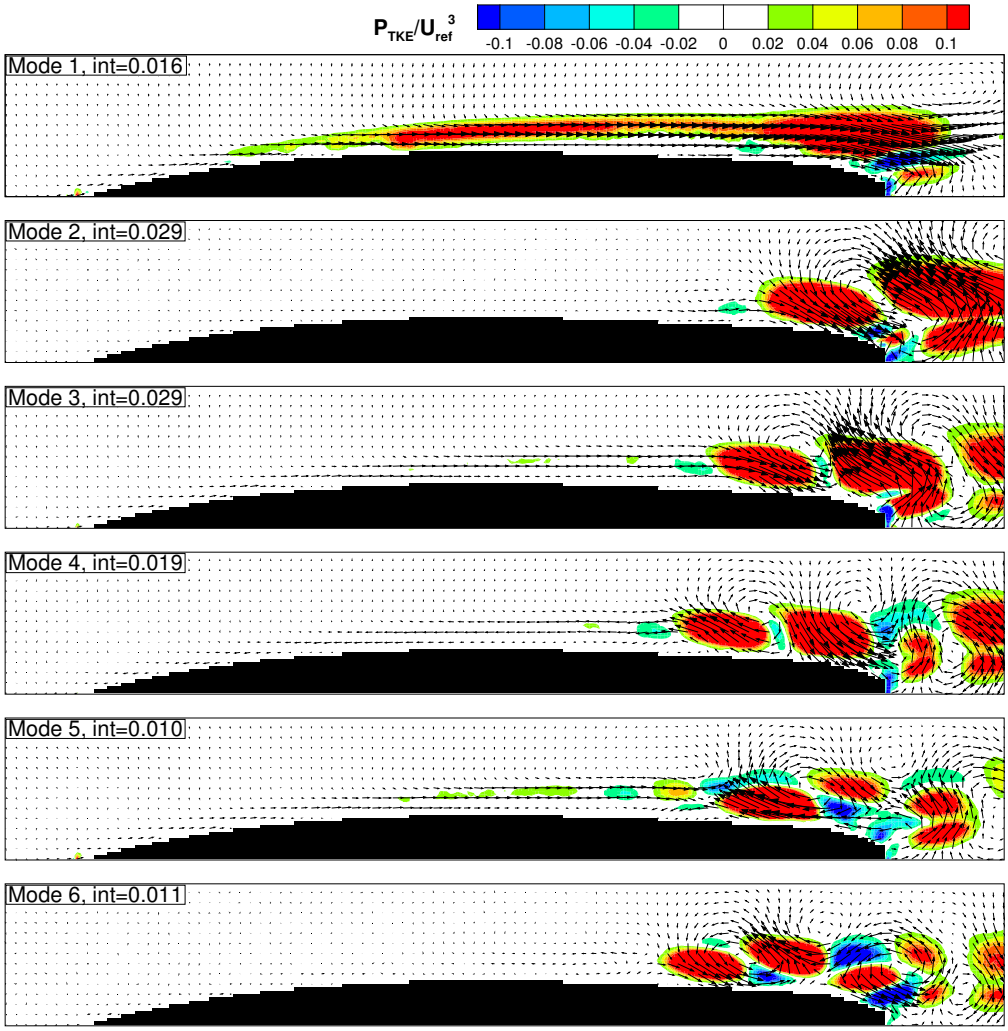

Figure 8: **TKE production rate per POD mode, steady case**

steady like state is able to develop, thus increasing the weight played by the boundary layer most energetic POD mode (which is now the second one). Results shown for the halved condition support the ability of POD in clearly recognizing and split with the relative weight the different phenomena that simultaneously act generating the complex unsteady flow field previously observed in Fig. 3.

Loss production analysis

As discussed in the previous sections, the POD can be used to represent and split, on a statistical basis, the structures that characterize the unsteady flow field according to their energy rank. However, as discussed in the data analysis section, the POD can be also used for a further analysis step. Each POD mode can be related to a quota of the TKE production rate and equivalently to the loss generation rate.

The following three figures (Figs. 8, 9, 10) represent for the three cases (steady, nominal and halved f^+, respectively) the production rate of TKE (P_{TKE}) per POD mode. This quantity has been normalized by the cube of the reference velocity and a unitary length. The integral value on the measurement domain has been also computed for each mode and it is indicated in the figures in order to provide the weight of the different phenomena in producing losses.

The production of TKE for the steady condition (Fig. 8) is mainly related to the Reynolds shear stresses caused by the vortical structures originating from the boundary layer separation, except for the first POD mode. The first mode, as previously observed, is related to low frequency fluctuations

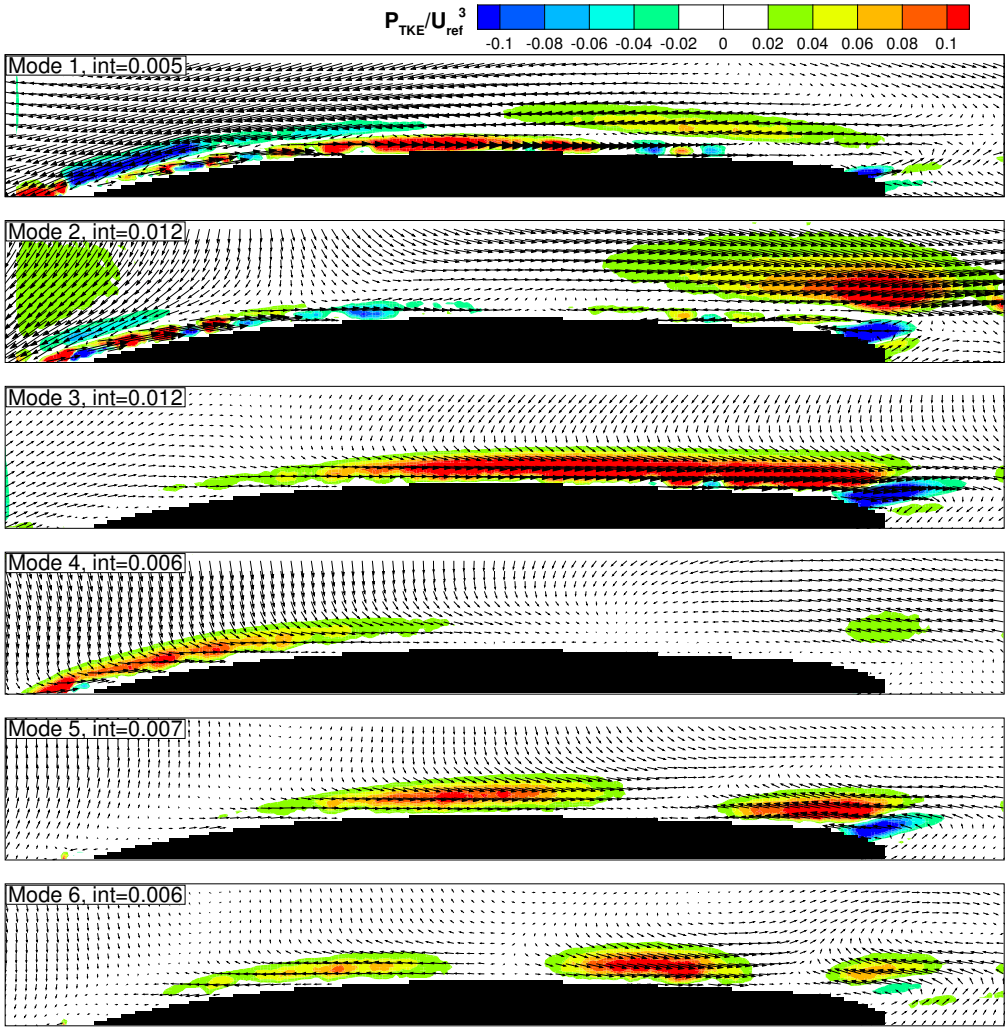

Figure 9: **TKE production rate per POD mode, nominal f^+ case**

of the whole boundary layer region due to streaky structures. However, the integral loss production rate of this mode is lower than that of the modes related to the vortical structures. As expected, for the steady case all the sources of losses are confined in the boundary layer region, with the greatest amount of losses due to the boundary layer separation.

The unsteady case with nominal f^+ (Fig. 9) presents a completely different scenario. The first two modes, related to the large scale structures of the wake, have a lower production rate of TKE with respect to the steady case (being representative of different dynamics). For these modes the largest production is found within the boundary layer in the region where the roll up vortices caused by the interaction of the wake leading boundary and the boundary layer were previously observed. Significant losses can also be observed in mode 2 at the edge of the boundary layer in the surround of the end of the profile surface. However, in the boundary layer region the contribution due to the wake related modes together (1 and 2) to the loss generation rate is lower than the contribution due to the boundary layer related events (modes above 2). Particularly, the third mode gives the largest production rate within the measurement domain. In this case no vortex like structures are responsible for these losses, according to the absence of separation. Moreover, in the unsteady case, loss generation rate due to the wake modes is not null in the potential flow region, outside the boundary layer. Thus, wake migration across the passage represents an additive source of losses characterizing the unsteady operation of the cascade, as also discussed in Michelassi et al (2015). Also regions of positive values of P_{TKE} appear in the plot. Here, the TKE is reconverted to mean flow energy.

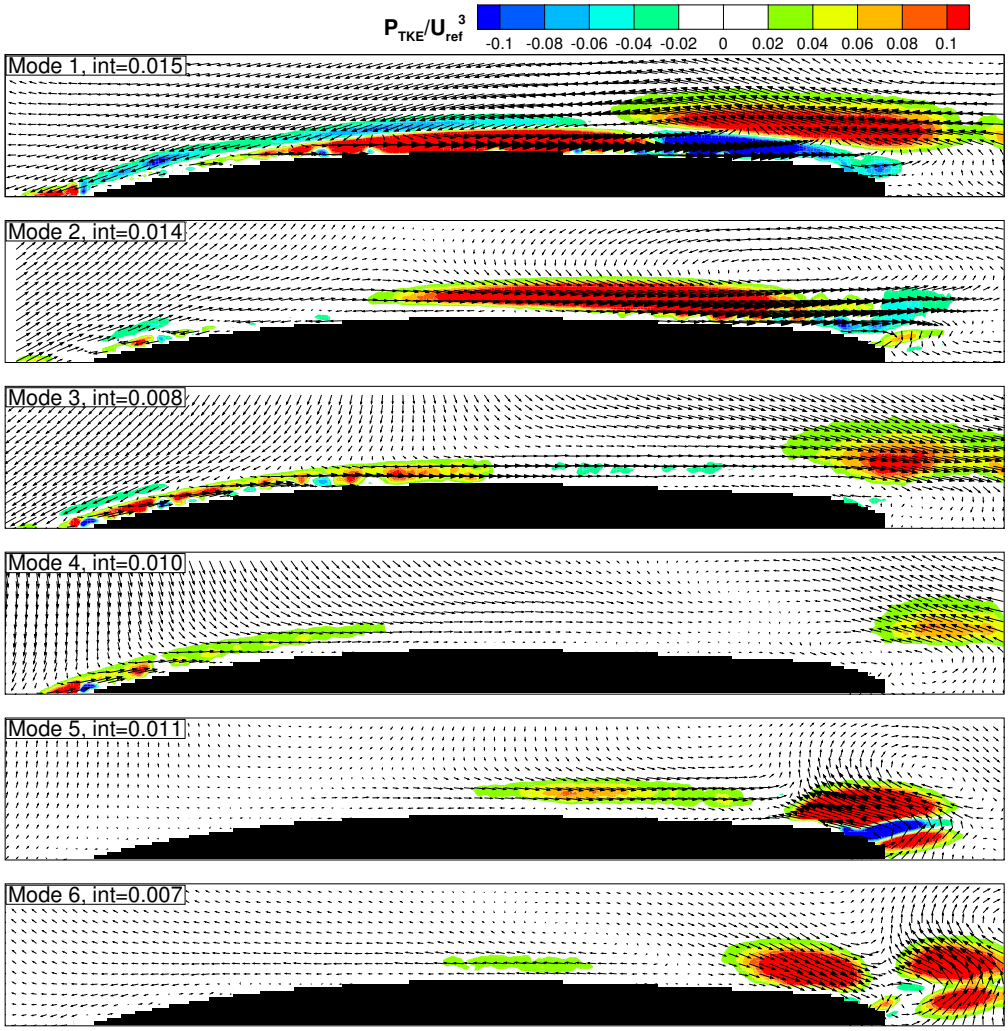

Figure 10: **TKE production rate per POD mode, halved f^+ case**

The halved f^+ case shows features of both the previously described cases. The TKE production rate distribution of modes 1, 3 and 4 is similar to that of mode 1, 2 and 4 of the nominal f^+ case. The loss generation rate (integrated value) related to the large scale structures of the incoming wake for the halved f^+ (modes 1 and 3) is higher than for the nominal case. This is because the roll-up vortex caused by the interaction of the wake and the boundary layer is larger for this condition, according to the thicker boundary layer developing between wakes (Satta et al, 2014). Mode 2 (the boundary layer mode) shows losses intermediate between their counterpart for the steady (mode 1) and the nominal unsteady case (mode 3). Modes 5 and 6 are instead related to the dynamics of the unsteady separation. The loss generation rate due to these modes is reduced for this unsteady case with respect to the steady one, according to the intermittent nature of the flow separation.

CONCLUSIONS

In the present work, POD has been applied to TR-PIV data in order to characterize the different phenomena responsible for loss generation. The ability of POD in highlighting the most important dynamics responsible for flow oscillations in the steady and in the unsteady cases has been highlighted by means of comparisons with time resolved and phase-averaged vector maps. In the steady case POD modes evidently represent the low frequency elongated oscillations as well as the vortical structures shed as a consequence of the boundary layer laminar separation occurring in this condition. For the unsteady cases the most energetic POD modes describe (statistically) the negative jet effects. The

combination of the first two modes reproduces the phase-averaged flow filed. The analysis of two different reduced frequency strengthens the ability of POD. Indeed, in the case of the halved reduced frequency POD modes have been shown to be able to capture superposed phenomena typical of both the steady and the unsteady operations, such as the wake migration and boundary layer separation induced effects. A loss split procedure, based on the bi-orthogonality condition of the POD modes and related temporal coefficients, allowed the quantification of the weight of each dynamics on the overall loss production rate. In the steady case losses are mainly due to the vortex shedding phenomenon, while in the unsteady case the rollup vortex generated during the wake-boundary layer interaction has been found to be the dynamics with higher losses. This latter appears sensibly influenced by the reduced frequency, with higher contribution for the halved reduced frequency condition due to a thicker boundary layer developing between wakes. Losses due to wake migration also affect the potential flow region. The clear identification of the dynamics, the estimation of their weight and the localization of the flow region where they act in producing losses may contribute in the future to the development of optimization strategies for high lift profile cascades operating under realistic unsteady flow conditions.

REFERENCES

Gompertz KA, Bons JP (2011) Combined unsteady wakes and active flow control on a low-pressure turbine airfoil. AIAA Journal of Propulsion and Power 27:990–1000

Hodson HP, Howell RJ (2005) The role of transition in high-lift low-pressure turbines for aeroengines. Prog in Aerospace Sci 41:419–454

Kurelek JW, Lambert AR, Yarusevych S (2016) Coherent structures in the transition process of a laminar separation bubble. AIAA Journal 54:2295–2309

Lengani D, Simoni D (2015) Recognition of coherent structures in the boundary layer of a low-pressure-turbine blade for different free-stream turbulence intensity levels. International Journal of Heat and Fluid Flow 54:1–13

Lengani D, Simoni D, Ubaldi M, Zunino P (2014) POD analysis of the unsteady behavior of a laminar separation bubble. Exp Therm Fluid Sci 58:70–79

Lengani D, Simoni D, Ubaldi M, Zunino P, Bertini F (2016) Coherent structures formation during wake-boundary layer interaction on a lp turbine blade. Flow, Turbulence and Combustion pp 1–25

Michálek J, Monaldi M, Arts T (2012) Aerodynamic performance of a very high lift low pressure turbine airfoil (t106c) at low reynolds and high mach number with effect of free stream turbulence intensity. Journal of Turbomachinery 134(6):061,009 1–10

Michelassi V, Chen LW, Pichler R, Sandberg RD (2015) Compressible direct numerical simulation of low-pressure turbines-part II: Effect of inflow disturbances. Journal of Turbomachinery 137(7):071,005 1–12

Pacciani R, Marconcini M, Arnone A, Bertini F (2012) Urans analysis of wake-induced effects in high-lift, low reynolds number cascade flows. In: ASME Turbo Expo 2012: Turbine Technical Conference and Exposition, pp 1521–1530

Sarkar S (2008) Identification of flow structures on a lp turbine blade due to periodic passing wakes. Journal of Fluids Engineering 130(6):061,103 1–10

Satta F, Simoni D, Ubaldi M, Zunino P, Bertini F (2014) Loading distribution effects on separated flow transition of ultra-high-lift turbine blades. AIAA J of Prop and Power 30:845–856